

## RESEARCH ARTICLE

# 4D Printing of Plasmon-Encoded Tunable Polydimethylsiloxane Lenses for On-Field Microscopy of Microbes

Stefano Mariani, Martina Corsi, Alessandro Paghi, Antonino A. La Mattina, Lucanos Strambini, Francesco P. Frontini, Graziano Di Giuseppe, and Giuseppe Barillaro\*

Here the 4D printing of a magnifying polydimethylsiloxane (PDMS) lens encoded with a tunable plasmonic rejection filter is reported. The lens is formed by moldless printing of PDMS pre-polymer on a nanostructured porous silicon (PSi) templating layer. A nanometer-thick plasmonic filter is integrated on the lens surface by in situ synthesis of Ag and Au nanoparticles (NPs) with programmed density. The filter can be designed to reject light at the plasmonic resonance wavelength of the NPs with an optical density tunable from 0 to 3 and retrieve light at longer wavelengths with a pass-to-stop band ratio tunable from 0 to 60 dB. Swelling of PDMS in hexane and ether is used to change the NP density on the lens surface and modulate, in turn, the transmittance properties of the NP-decorated lens over 3 orders of magnitude. The plasmon-encoded lens is coupled to a commercial smartphone demonstrating: shaping of the emission spectrum of a white light-emitting diode to tune the color from yellow to purple; real-time bright-field and fluorescence microscopy of living microbes in water, namely, the auto-fluorescent green alga *Chlorogonium* sp. and the ciliated protozoan *Euplotes daidaleos*.

handheld, and in field-portable, enabling a spatiotemporal mapping of the microbiome potentially leading to unprecedented insight into human health and environment conditions.<sup>[1]</sup>

Smartphone-based optical/fluorescence microscopy leverage the scaling down of lens/filter optical components and the computational/networking capabilities of smartphones.<sup>[1–4]</sup> These platforms have proved to be very effective for biomedical applications. Nonetheless, the cost of manufacturing of miniaturized optical components, i.e., the lenses and filters, for the assembling of add-on optical modules for smartphones with reduced size and weight (yet, hundreds of grams and of cm<sup>3</sup>) has hampered the diffusion of smartphone-based microscopy to date.<sup>[5]</sup>

To circumvent these limitations researchers have developed strategies to fabricate polymeric (e.g., polydimethylsiloxane, PDMS) magnifying lenses that can be directly attached to the smartphone camera to boost intrinsic magnification and resolution performance.<sup>[6–8]</sup> These strategies include hanging droplet of uncured PDMS deposited by inkjet printing on heated flat surface;<sup>[6]</sup> moldless thermal curing of PDMS droplet prepared using a moving needle extruder;<sup>[7]</sup> drop-casting of uncured PDMS droplet onto a smooth circular disk of poly(methyl methacrylate);<sup>[8]</sup> moldless printing of uncured PDMS droplet using nanostructured porous silicon (PSi) as templating layer.<sup>[5]</sup>

In two cases the polymeric lens also embedded a rejection optical filter that enabled performing smartphone-based fluorescence microscopy leveraging image magnification and light rejection properties of the lens.<sup>[5,9]</sup> In Ref. [9], the lens-filter element was prepared mixing PDMS prepolymer with dyes featuring high absorbance in specific wavelength regions. The lens was coupled to a smartphone and used in several bioanalytic applications, namely, cell and tissue observation, cell counting, and plasmid transfection evaluation.<sup>[9]</sup> In Ref. [5], a nanostructured porous silicon oxide (PSiO<sub>2</sub>) filter, namely, a distributed Bragg reflector (DBR) with stopband tuned to reject light in a selected wavelength region, was integrated into the PDMS lens. The lens-filter element was coupled to a smartphone and used for the fluorescence imaging and counting of CAOV-3 ovarian cancer cells in a conventional live/dead assay.<sup>[5]</sup>

Very recently our research group developed a fluoride-assisted chemical route for the in-situ synthesis of metal nanoparticles (NPs) on PDMS.<sup>[10]</sup> In contrast to conventional in

## 1. Introduction


Smartphone-based microscopy represents a powerful tool for studying the composition of the environmental microbiome, though not limited to.<sup>[1]</sup> Compared to conventional bulky and expensive instrumentation, these platforms are cost-effective,

S. Mariani, M. Corsi, A. Paghi, A. A. La Mattina, G. Barillaro  
Department of Information Engineering  
University of Pisa

Via G. Caruso 16, Pisa 56122, Italy  
E-mail: giuseppe.barillaro@unipi.it

L. Strambini, G. Barillaro  
Institute of Electronics, Information Engineering  
and Telecommunications  
National Research Council  
Via G. Caruso 16, Pisa 56122, Italy

F. P. Frontini, G. D. Giuseppe  
Department of Biology  
University of Pisa  
Via L. Ghini 13, Pisa 56126, Italy

 The ORCID identification number(s) for the author(s) of this article can be found under <https://doi.org/10.1002/adom.202101610>.

© 2021 The Authors. Advanced Optical Materials published by Wiley-VCH GmbH. This is an open access article under the terms of the Creative Commons Attribution License, which permits use, distribution and reproduction in any medium, provided the original work is properly cited.

DOI: 10.1002/adom.202101610

situ synthetic approaches that result in relatively poor surface decoration over hours to days,<sup>[11]</sup> in Ref. [10] we demonstrated that the addition of fluoride ions to a metal solution speeds up the metal ions reduction process at the PDMS surface by two orders of magnitude enabling to coat the surface with plasmonic metal nanoparticles (i.e., Ag, Au) in few minutes.<sup>[10]</sup>

Here we report on the 4D printing, i.e., 3D printing with reversible shape, property, and functionality,<sup>[12,13]</sup> of magnifying PDMS lenses encoded with a tunable plasmonic filter. The lens is moldless printed using PDMS pre-polymer on a nanostructured porous silicon templating layer. A nanometer-thick plasmonic filter is integrated on the PDMS lens surface by in-situ fluoride-assisted synthesis of Ag and Au NPs. The filter transmittance at the plasmonic resonance wavelength can be controlled over a factor 1000 by tuning the NP density on the lens surface during the synthetic process, thus enabling to vary the optical density (OD) from 0 to 3 and extinction pass-to-stop band ratio (ER) from 0 to 60 dB. Swelling of PDMS in hexane and diethyl ether can be further used to decrease the NP density on lens surface after fabrication and increase, in turn, the filter transmittance at the plasmon resonance wavelength of about 3 orders of magnitude, thus enabling to dynamically tune OD from 3 to 0.3. As proof of concept application in lightining and microscopy, we coupled the plasmon-encoded lens to a commercial smartphone demonstrating: shaping of the emission spectrum of a commercial white light emitting diode (LED) and, in turn, color tuning from yellow to purple; real-time bright-field and fluorescence microscopy of living microbes in water, namely, the auto-fluorescent green alga *Chlorogonium* sp. and the ciliated protozoan *Euplotes daidaleos*. These organisms, in addition to having a high evolutionary importance (they are considered the ancestors of all higher multicellular organisms, such as plants, animals, and fungi), they are indicators of the quality of the environment as well as being of impressive health interest (the parasitological type are the infectious agents of very serious diseases, such as malaria, toxoplasmosis, and leishmaniasis).<sup>[14]</sup>

## 2. Results and Discussion

**Figure 1a** shows a sketch of the main steps involved in the preparation of the plasmon-encoded PDMS lens. The PDMS lens is moldless-printed on a nanostructured porous silicon (PSi) templating layer featuring randomly-arranged cylindrical pores with size and length of about 50 nm and 10  $\mu\text{m}$ , respectively, and porosity tuned from 59% to 77% (Figure S1, Supporting Information).<sup>[5]</sup> SEM top-view and cross-section images of the templating PSi layer with porosity of 77% are given in Figure S1 (Supporting Information). A calibrated droplet (10 mg) of PDMS pre-polymer is printed onto the PSi surface using a small nozzle. Once it contacted the PSi surface the PDMS droplet formed an oblate spheroid cap due to the balance of adhesive and cohesive forces involved in surface wetting and gravity (Bond number  $B_0 = 0.81$ ).<sup>[15,16]</sup> Upside-down curing of the droplet resulted in a PDMS lens with prolate spheroid shape. Optical images of the lens after upside-down curing are provided in Figure 1b. The PDMS lens was then easily peeled off the host PSi layer, thus

achieving a free-standing silicone lens retaining both mechanical and optical characteristics of PDMS.

Figure 1c–f and Figure S2 (Supporting Information) summarize geometrical (i.e., diameter, height, apex curvature radius) and optical (i.e., focal length, numerical aperture, spherical aberrations) properties of bare PDMS lenses. The lenses have average width and height of 3.3 and 2 mm, respectively, slightly depending on the porosity of the templating layer (Figure 1c). The focal length ( $f$ ) and numerical aperture (NA) of the lenses increased from 2.53 to 2.96 mm and from 0.32 to 0.36 with the porosity of the templating layer (Figure 1e,f), whereas the spherical aberrations reduced as the porosity of the templating layer increased, thus improving fidelity of images acquired with lenses with longer focal length (Figure S2g–i, Supporting Information). The average %RSD values were all around 5% or below both for geometrical and optical parameters, thus confirming the excellent reproducibility and controllability of the lens formation process. Namely, %RSD = 2.9% for diameter, 2.3% for height, 2.7% for curvature radius, 6.6% for focal length, and 4.3% for the numerical aperture were achieved.

We characterized the bare PDMS lens in a set of high-resolution imaging tests. For these experiments we used the lens with focal length of 2.82 mm due to the reduced spherical aberrations and improved image fidelity (Figure S2, Supporting Information). The lens was firmly, though reversibly (>100 times), attached to the built-in camera of a commercial smartphone thanks to the excellent adhesion properties of PDMS to glass surfaces, as sketched Figure 1g. Figure 1h shows a picture of a chromium-on-quartz test pattern containing parallel lines with width sequentially reducing from 30 to 4  $\mu\text{m}$  (constant duty-cycle of 0.5) acquired using the lens-smartphone system; the control image acquired with the bare smartphone camera (i.e., without the PDMS lens) at the maximum allowable digital magnification (4 $\times$ ) is also given for comparison (Figure 1i). All the micrometric lines were clearly resolved with signal-to-noise ratio (SNR) of about 10 and 100 for 4 and 30  $\mu\text{m}$ -wide lines, respectively (Figure 1j); no line distortion was evident, confirming high magnification and low aberrations of the lenses when operated in convex-plano mode. As a benchmark of the quality of images acquired with the lens-smartphone system, we used a commercial microscope to acquire control images of the test pattern of Figure 1h with comparable magnification. We then compared the signal-to-noise ratio measured on the images acquired with both the systems. Despite the obvious superiority of the commercial microscope in terms of resolution, image contrast, and fidelity, the lens-smartphone system performed surprisingly well considering its cost, portability, and ease of use (Figure S3a,b, Supporting Information).

We next decorated the bare lens with Ag and Au NPs by immersion in an ethanolic solution of  $15 \times 10^{-3}$  M AgF or HAuCl<sub>4</sub>:NH<sub>4</sub>F, respectively, for different times (Figure 2a). This enabled to incorporate in the lens a plasmonic filter rejecting light around 400 and 530 nm for Ag and Au NPs, respectively.<sup>[10]</sup> The PDMS lens appeared brownish after decoration with Ag and violet after decoration with Au, with color intensity increasing with the decoration time. This was ascribed to localized surface plasmon resonance (LSPR) absorption of the NPs that increased with the NP density and/or surface coverage as the immersion time increased.<sup>[10]</sup>

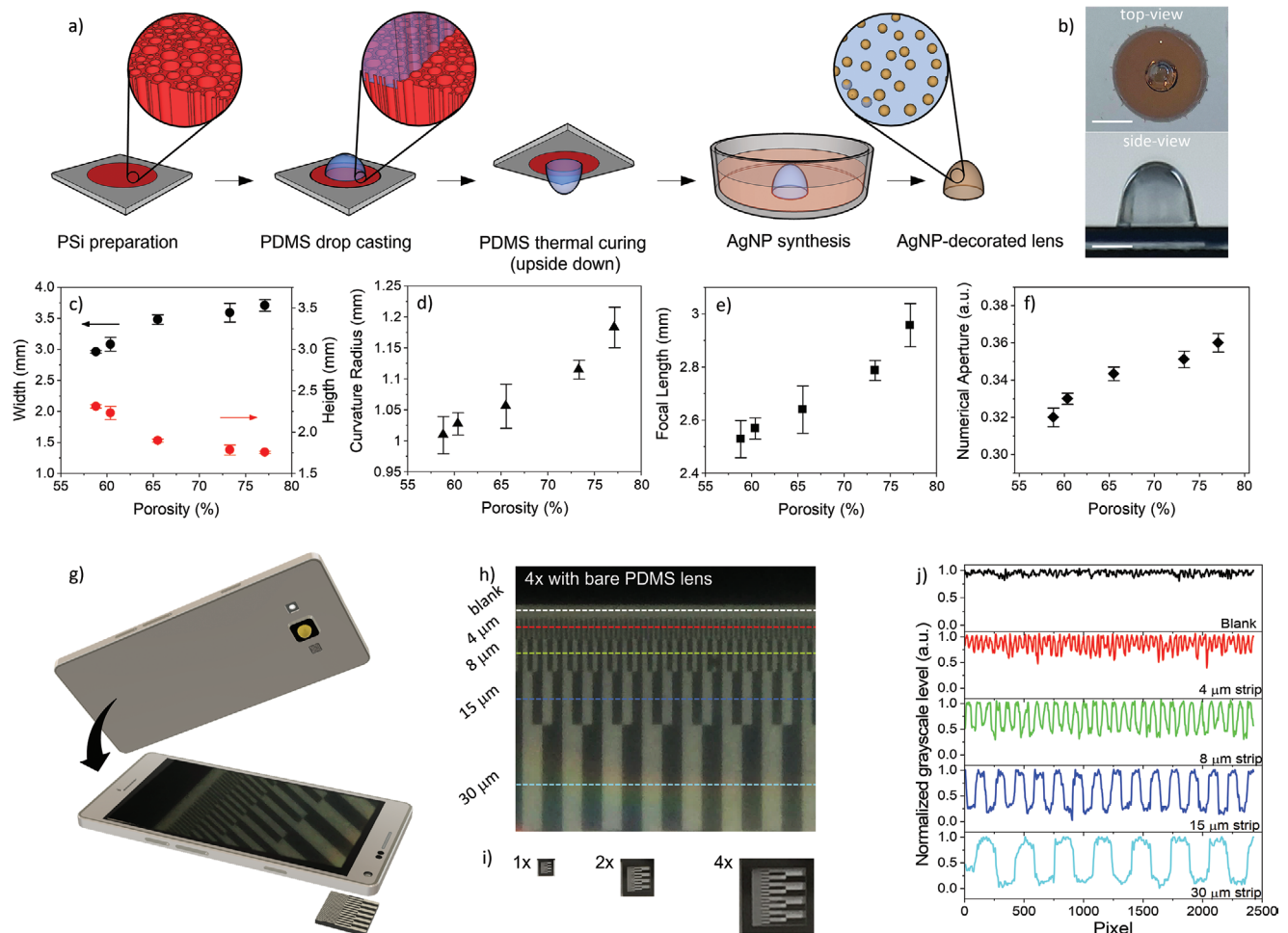


**Figure 1.** Preparation and characterization of PDMS lenses moldless-printed on a nanostructured porous silicon templating layer. a) Sketch of the moldless printing fabrication of a magnifying PDMS lens with different focal lengths from 2.5 to 2.8 mm, embedding an AgNP and/or AuNP plasmonic filter. b) Top-view and side-view of a PDMS lens standing on a PSi templating layer after upside-down curing. Markers are 5 mm (top) and 1 mm (bottom). c–f) Geometrical and optical properties of PDMS lenses (10 mg) prepared onto PSi templating layers with porosity of 58.8 ± 0.4%, 60.4 ± 0.1%, 65.5 ± 0.1%, 73.3 ± 0.5%, and 77.1 ± 0.2%, respectively. The error bars represent one standard deviation with respect to average values achieved over a number of 3 samples per each porosity. g) Sketch of a smartphone coupled with a PDMS lens for imaging applications. h) Pictures of a chromium-on-quartz test pattern containing lines of width ranging from 250 to 4 μm with constant duty cycle of 0.5, acquired with a PDMS lens with focal length of 2.8 mm adhered to the camera of a commercial smartphone, at 4× digital zoom. i) Pictures of the test pattern in (h), captured with the as-received commercial smartphone using 1×, 2×, and 4× digital zoom. j) Grayscale intensity profiles of the lines in (h), from which it is apparent that lines with width down to 4 μm can be resolved (S/N ratio ≈ 10).

SEM analysis of the PDMS lenses decorated in ethanolic solution of  $15 \times 10^{-3}$  M AgF for 1, 4, and 9 min confirmed the presence of AgNPs on the lens surface (Figure 2b). Density, size distribution, and surface coverage of the AgNPs changed as the decoration time increased. The density of the AgNPs onto the PDMS surface increased from  $53 \pm 2$ , to  $60 \pm 13$ , and  $116 \pm 13$  NPs  $\mu\text{m}^{-2}$  for decoration times of 1, 4, and 9 min, respectively (Figure 2c). The average size of the AgNPs also increased with time, from  $9.9 \pm 3.4$ , to  $12.0 \pm 4.2$ , and  $14.0 \pm 4.7$  nm (Figure S4a, Supporting Information), as well as the surface coverage, from  $2.7 \pm 0.5$ ,  $3.2 \pm 1.1$ , and  $5.4 \pm 1.7\%$  (Figure S4b, Supporting Information).

Figure 2d shows the transmission spectra of PDMS lenses decorated with AgNPs for 1, 4, and 9 min. The lenses feature a long-pass transmission spectrum with passband at wavelengths

>500 nm and stopband centered at 403 nm, i.e., at the LSPR wavelength of AgNPs. A clear transmittance dip at 403 nm appeared after 1 min of decoration, which is consistent with the LSPR peak of AgNPs grown on the lens surface; the transmittance at the plasmonic resonance wavelength further reduced with the decoration time, reaching a value of about 0.1% after 9 min. OD and ER values of the 9-min-decorated lens were about 3 (at 403 nm) and 60 dB, respectively (Figure 2e), meaning that light at the plasmonic resonance wavelength is attenuated of a factor 1000, while longer wavelengths (>500 nm) are readily transmitted through the lens. Similarly, the presence of AuNPs on the lens surface synthesized in a  $15 \times 10^{-3}$  M HAuCl<sub>4</sub>:NH<sub>4</sub>F ethanolic solution was corroborated by the occurrence of a plasmonic resonance peak at 530 nm (Figure S5a, Supporting Information). The transmittance value at the plasmonic resonance wavelength



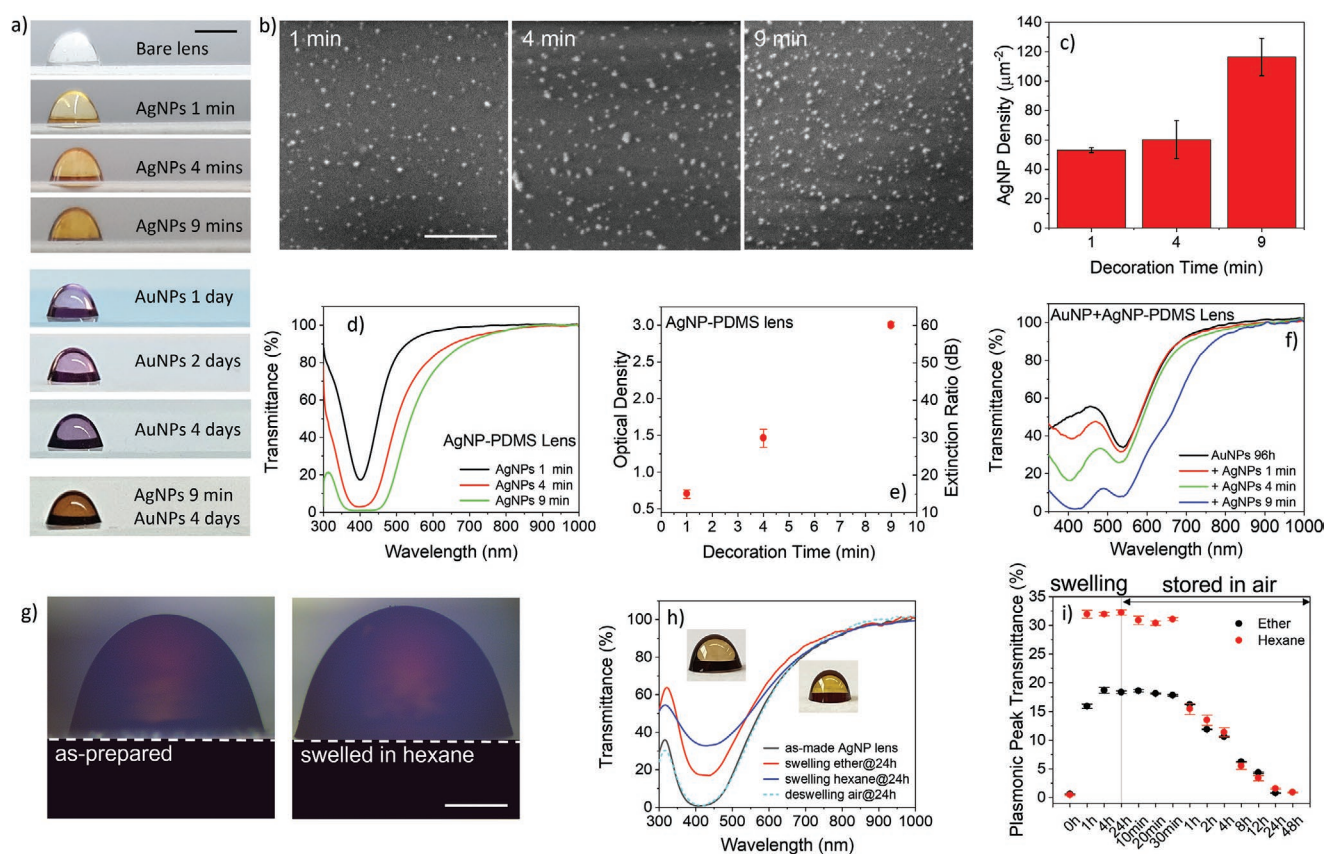


**Figure 2.** Optical and morphological characterization of 4D printed plasmon-encoded PDMS lenses. a) Pictures of PDMS lenses before decoration (bare, top), after decoration with AgNPs in an ethanolic solution of  $15 \times 10^{-3}$  M AgF for 1, 4, and 9 min, after decoration with AuNPs in an ethanolic solution with  $15 \times 10^{-3}$  M  $\text{HAuCl}_4 \cdot \text{NH}_4\text{F}$  for 1, 2, and 4 days, and after decoration with both AuNPs for 4 days and AgNPs for 9 min. Scale bar is 3 mm. b) SEM images of AgNPs on the surface of PDMS lenses decorated in an ethanolic solution of  $15 \times 10^{-3}$  M AgF for 1, 4, and 9 min. Scale bar is 500 nm. c) NP density on PDMS lenses decorated with AgNPs as reported in (a). d) Transmittance spectra of PDMS lenses decorated with AgNPs as reported in (a). e) Experimental OD and ER values measured at 403 and 635 nm on PDMS lenses decorated with AgNPs, synthesized in an ethanolic solution of  $15 \times 10^{-3}$  M AgF for 1, 4, and 9 min. f) Transmittance spectra of a PDMS lens decorated with AuNPs upon immersion for 96 h in an ethanolic solution of  $15 \times 10^{-3}$  M  $\text{HAuCl}_4 \cdot \text{NH}_4\text{F}$  and then decorated with AgNPs upon immersion for 1, 4, and 9 min in an ethanolic solution of  $15 \times 10^{-3}$  M AgF. g) Pictures (acquired in air) of a PDMS lens decorated with AgNPs ( $15 \times 10^{-3}$  M AgF in ethanol for 9 min) as-prepared and after 24 h swelling in hexane. Scale bar is 1 mm. h) Transmittance spectra (acquired in air) of a PDMS lens decorated with AgNPs ( $15 \times 10^{-3}$  M AgF in ethanol for 9 min) as-prepared, after 24 h of dipping (swelling) in diethyl ether and hexane, and after 24 h of drying (deswelling) in air. i) Swelling/deswelling kinetics of an AgNP-PDMS lens measured in air after immersion in hexane and diethyl ether up to 24 h, then stored in air up to 48 h. The transmittance value at the plasmonic peak wavelength is used as the parameter of merit.

reduced as the immersion time increased (1h-96h), consistently with the increased AuNP density/coverage on the PDMS lens.

The proposed approach permits to synergistically combine different metal NPs on the same PDMS lens through successive synthetic steps. Here we demonstrate the combination of both Au and Ag NPs on a single PDMS lens (Figure 2a, bottom). Figure 2f shows the transmittance spectrum of a lens firstly decorated with AuNPs for 96 h, then decorated with AgNPs for different times (i.e., 1, 4, and 9 min). The effect of both Ag and Au NPs on the transmittance spectrum of the hybrid Ag/AuNP lens can be distinctly appreciated. The transmittance spectrum of the hybrid lens is consistent with the superposition of the spectra of AuNP and AgNP PDMS lenses. Sample-to-sample reproducibility of the multi-material lens fabrication is excellent (Figure S5b, Supporting Information).

We then investigated dynamic tuning (4D features) of the transmittance spectrum of NP-decorated lenses leveraging the

reversible swelling of PDMS in solvents, namely, hexane and diethyl ether.<sup>[17]</sup> AgNP-decorated PDMS lenses ( $15 \times 10^{-3}$  M AgF 9 min) were dipped in pure diethyl ether and hexane for different times, from 1 to 24 h (Figure 2g,h and Figure S6a, Supporting Information). The lens volume increased upon immersion in the solvents, in agreement with the swelling ratio of PDMS in diethyl ether and hexane,<sup>[17]</sup> reaching a steady state value after 1 h. Remarkably, the lens swelling was retained in air for about 30 min after extraction of the lens from the solvents, which permitted to measure size and transmittance changes of the lens upon swelling. A uniform swelling ratio, i.e.,  $\%(L_{\text{swell}} - L_0)/L_0$ , of about 10% and 8% was measured in air after immersion of the lens in hexane and diethyl ether, respectively. Consistently, the transmittance value of the swelled lens at the LSPR wavelength increased up to a factor 1000, compared to that of the as-prepared lens, due to the decreased surface density of AgNPs upon swelling (Figure 2h, Figure S6c,d,

Supporting Information). The larger the swelling ratio the higher the transmittance value at the LSPR wavelength of the lens after immersion in the solvents, namely, about 32% and 19% in hexane and diethyl ether, respectively. This agrees well with the transmittance value at the LSPR wavelength of AgNP-PDMS lenses prepared at different synthesis times and, in turn, with different surface densities (Figure 2c,d). The swelling process is fully reversible. Both size and transmittance of the lens return back to those of the as-prepared lens (i.e., before immersion in solvents) after 24 h of storage in air, due to complete evaporation of the solvents (Figure 2h,i and Figure S6e,f, Supporting Information). Figure 2i shows the swelling/de-swelling kinetics of an AgNP-PDMS lens measured in air after immersion in hexane and diethyl ether for 24 h, then stored in air for 48 h, using the transmittance value at the plasmonic resonance wavelength as the parameter of merit. A 30-min-large interval with stable transmittance value is evident after swelling, during which the swelled lens can be used for quasi-neutral imaging purposes leveraging the 1000 times higher transmittance value at the LSPR wavelength.

The ability of PDMS lenses decorated with AgNPs and AuNPs to filter light with high spectral fidelity led us to explore their use in lighting applications.<sup>[5]</sup> We found that the colour of a commercial white LED could be adjusted by the appropriate decoration with plasmonic NPs. For this configuration, the PDMS lens (with/without NPs) was placed on top of the LED of a commercial smartphone and the spectrum

of the light transmitted through the lens was acquired by a spectrometer (Figure 3a). The emission spectrum of the bare LED (i.e., without lens) was used as the reference spectrum; the emission spectrum of the LED coupled to a bare PDMS lens was used as the control spectrum (Figure 3b). Transmission spectra of the AgNP-decorated lenses and emission spectra of the LED acquired through these lenses are reported in Figure 3c and 3d, respectively. The emission spectra in Figure 3d show that the plasmonic filter embedded in the lens attenuates intensity of the LED emission at specific wavelength intervals (i.e., those falling in LSPR absorption region) providing a simple and effective approach to shape the color of light transmitted through the lens. Data from representative samples are shown superimposed on a CIE 1931 diagram in Figure 3e.

We next investigated the capability of AgNP-decorated lenses in fluorescence imaging applications. A 9-min-decorated AgNP-PDMS lens with focal length of 2.8 mm was attached to the camera of a commercial smartphone, then the lens-smartphone system was used to image fluorescent polyethylene microbeads (emission  $\lambda_{em} = 515$  nm, excitation  $\lambda_{ex} = 403$  nm, 448 nm) (Figure S7a,b, Supporting Information) with diameter of 53–63  $\mu\text{m}$  (Figure S8, Supporting Information). The bare PDMS lens (i.e., before AgNP decoration) and the naked smartphone (i.e., without lens) were used to acquire control images of the beads (Figure S9, Supporting Information). Quality of fluorescence images acquired with the lens-smartphone system

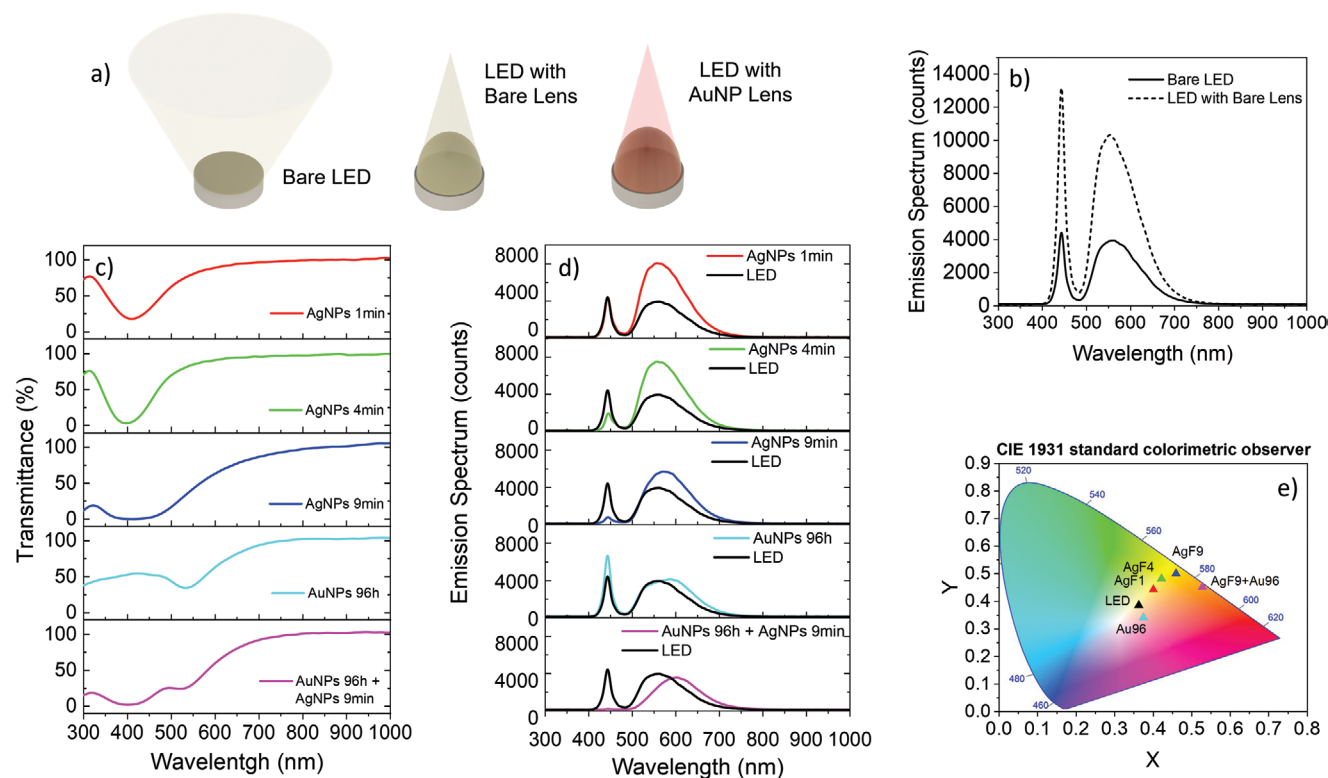


**Figure 3.** Lighting application of the PDMS lens decorated with AgNPs and/or AuNPs coupled to a white commercial LED. a) Sketch of the experimental configuration for the lighting application test. b) Emission spectra of a commercial white LED with/without a bare lens. c) Transmittance spectra of the PDMS lenses decorated with: AgNPs for 1, 4, and 9 min; AuNPs for 96 h; AgNPs for 9 min + AuNPs for 96 h. d) Emission spectrum of the bare white LED (black trace) superimposed to spectra of the LED coupled with PDMS lenses decorated with AgNPs and AuNPs as in (c). e) Spectral data from (d) represented in a CIE 1931 diagram of the colour perceived by the human eye.

was excellent, thanks to the high magnification and low spherical aberrations of the lens coupled with the excellent rejection (OD = 3) of the excitation light at 403 nm and effective retrieving of the beads green fluorescence (ER = T515/T403 = 51 dB).

As a proof-of-concept application, we tested the lens-smartphone system in the real-time imaging of living unicellular organisms in water, namely, the ciliated protozoan *E. daidaleos* and the green alga *Chlorogonium* sp. *E. daidaleos* is a protist with a size of 77–119  $\mu\text{m}$  in body length and 43–80  $\mu\text{m}$  in body width<sup>[18]</sup> (Figure S10, Supporting Information), and high motility. It is also the only species of *Euplotes* that lives in endosymbiosis with auto-fluorescent “*Chlorella*” like green algae. The green alga *Chlorogonium* is an auto-fluorescent alga (at 680 nm) often used for nutrition of freshwater heterotrophic protists. The species of genus *Chlorogonium* have an average size of about 34  $\mu\text{m}$  in body length and 4.8  $\mu\text{m}$  in body width (Figure S10a, Supporting Information).<sup>[19]</sup> These organisms have been assessed as important indicators of the quality of the environment (bioindicator) as well as being of impressive interest for the detection of important diseases (the parasitological type are the infectious agents of diseases, such as malaria, toxoplasmosis, and leishmaniasis).<sup>[14]</sup>

We firstly characterized the lens-smartphone system in bright-field microscopy experiments with *E. daidaleos*. A drop of *E. daidaleos* dispersion (10  $\mu\text{L}$ ) was placed on a glass slab and the system was used to monitor in real-time the living unicellular organisms in the drop (Figure 4a,b; Movie S1, Supporting Information). The imaging allowed to clearly appreciate single

unicellular organisms moving freely in the drop; remarkably, by using the 4 $\times$  digital zoom available in the smartphone the lens further enabled to appreciate some details of the inner fine structure of the ciliated protozoan, without any further image processing.

We next explored fluorescence microscopy capability of the system in a series of experiments involving the auto-fluorescence of the green alga *Chlorogonium* sp. (Figure S11a, Supporting Information), under laser excitation at 403 nm (Figure 4c–e). The images/movies acquired with the lens-smartphone system on 10  $\mu\text{L}$  of the algal dispersion dropped on a glass slab allowed to clearly appreciate the auto-fluorescence of single unicellular organisms gently floating in the drop (Figure 4d,e and Movie S2, Supporting Information). The AgNP-decorated lens fully removed the excitation light thanks to the high optical density OD = 3 at 403 nm, effectively retrieving the red auto-fluorescence ( $\approx 700$  nm) of the algal cells thanks to the high extinction ratio ER = 60 dB. Control images acquired with the smartphone equipped with the bare lens are reported in Figure S11b (Supporting Information); the excitation laser light leaks through the PDMS lens in absence of the AgNP plasmonic filter, significantly reducing the imaging performance. The lens-smartphone system also enabled counting the green alga *Chlorogonium* sp. cells per unit area both for the as-prepared solution ( $193 \pm 19$  cell  $\text{mm}^{-2}$ ) and at different dilution factors, namely, 0.5, 0.25, and 0.1 ( $21 \pm 6$  cell  $\text{mm}^{-2}$ ) (Figure 4f, Figure S11c,d, Supporting Information). The linearity ( $R^2 = 0.999$ ) achieved between cell density and dilution factor was excellent.

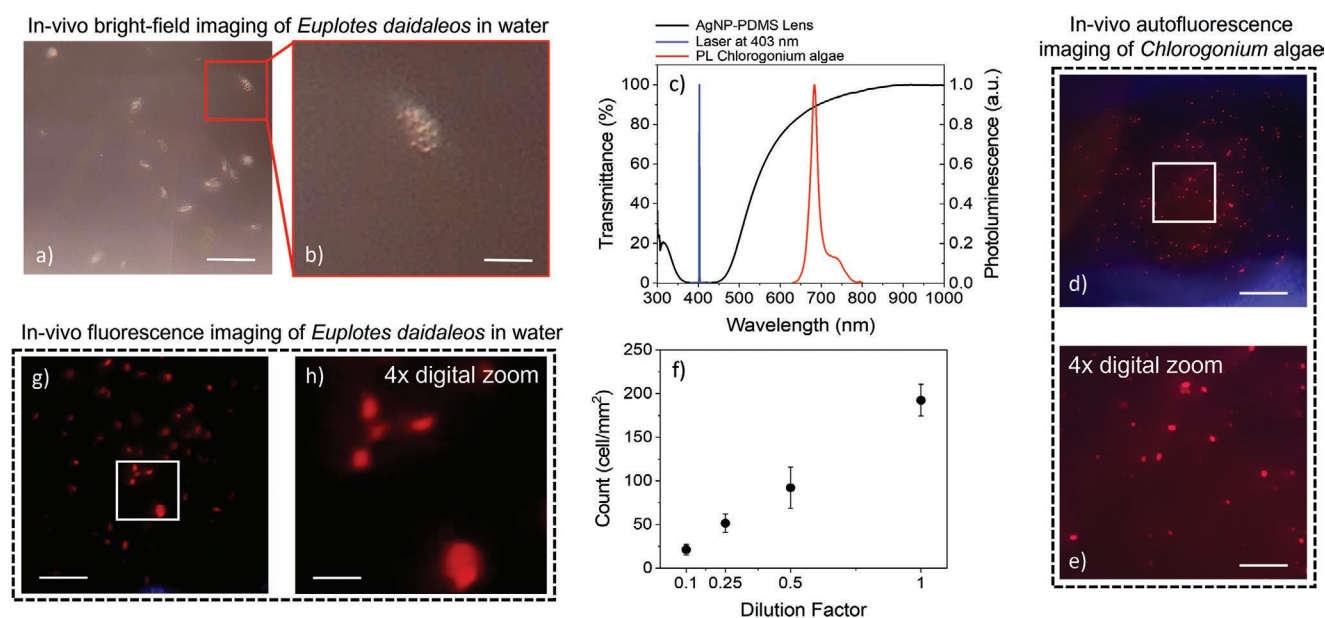


**Figure 4.** In vivo bright-field and fluorescence smartphone microscopy of auto-fluorescent unicellular microorganisms in a drop of water. a,b) Bright-field pictures at different magnifications of living *Euplotes daidaleos* in water acquired with a commercial smartphone equipped with a PDMS lens decorated with AgNPs for 9 min in an ethanolic solution of  $15 \times 10^{-3}$  M AgF. Scale bars in (a) and (b) are 200 and 50  $\mu\text{m}$ , respectively. c) Transmission spectrum (black trace) of the AgNP-decorated PDMS lens (OD = 3, ER = 60 dB) and photoluminescence spectrum (red trace) of *Chlorogonium* algae excited with a blue laser at 403 nm (blue trace). d,e) Fluorescence pictures of *Chlorogonium* algae in water acquired with the lens-smartphone system, upon excitation with a blue laser at 403 nm. Scale bars in (d) and (e) are 200 and 50  $\mu\text{m}$ , respectively. f) Cell density (cells  $\text{mm}^{-2}$ ) versus dilution factor of *Chlorogonium* algae as resulting from fluorescence images acquired using the lens-smartphone system. g,h) Fluorescence pictures of living *Euplotes daidaleos* after phagocytosis of *Chlorogonium* algae, acquired with the lens-smartphone system upon excitation with a blue laser at 403 nm. Scale bars in (g) and (h) are 200 and 50  $\mu\text{m}$ , respectively.



Eventually, we investigated fluorescence imaging of living *E. daidaleos* after phagocytosis of *Chlorogonium* algal cells. Thanks to the transparent body of these protozoa it is possible to observe the red fluorescence of algae, both of the endosymbiotic “*Chlorella*” like ones and of that of *Chlorogonium* cells ingested for phagocytosis, and to track down, in turn, the ciliated protozoan after phagocytosis. A volume of 10  $\mu$ L of *E. daidaleos* dispersion containing the algal cells was dropped on a glass slab and the lens-smartphone system was used to monitor the living organisms. Single protozoan organisms characterized by higher motility after phagocytosis were clearly observed by acquisition of the auto-fluorescence emission of the ingested algae, clearly distinct from unicellular algal organisms freely floating in the drop (Movie S3, Supporting Information). Figure 4g,h shows images extracted from Movie S3 (Supporting Information), where several red-fluorescent *E. daidaleos* after *Chlorogonium* cell ingestion were captured. Control fluorescence images/movies of the *E. daidaleos* after phagocytosis of the green alga *Chlorogonium* acquired with smartphone equipped with the bare PDMS lens and with the as-received smartphone (i.e., without the PDMS lens) are reported in Figure S12a,b and Movie S4 (Supporting Information); imaging of *E. daidaleos* before alga phagocytosis used as control experiment is reported in Movie S5 (Supporting Information).

### 3. Conclusions

In this work we reported on the 4D printing of magnifying, lightweight, self-adhesive PDMS lenses embedding a plasmonic filter with transmittance tunable in real-time upon immersion of the lens in a solvent. The lens is achieved through the mold-less printing of PDMS on a nanostructured PSi templating layer; the lens surface is then decorated with Ag and Au NPs synthesized in-situ with programmed density. The metal NPs on the lens surface encode a plasmonic filter featuring a rejection band at the LSPR wavelength of Ag and Au NPs with tunable transmittance depending on the NP density. The transmittance value of the plasmonic filter at the LSPR wavelength can be pre-designed in the fabrication phase with OD value from 0 to 3; this latter can be dynamically tuned from 3 down to 0.3 (a factor about 1000) in the operation phase upon immersion of the lens in hexane and ether, leveraging the controlled and reversible swelling of PDMS in solvents. As a proof-of-concept application in lighting and microscopy, we coupled the plasmon-encoded lens to a commercial smartphone to demonstrate color tuning of the light emitted by a white LED from yellow to purple, as well as real-time bright-field and fluorescence imaging of living microorganisms in water, namely, the auto-fluorescent green alga *Chlorogonium* sp. and the ciliated protozoan *E. daidaleos*.

The proposed 4D printing approach of NP-decorated PDMS lenses is immediately extendable to other metal nanoparticles, besides Ag and Au NPs, which can be also co-synthesized on the lens surface; the shape of NPs on the lens can be engineered to tune the plasmonic filter characteristics, such as resonance wavelength and quality factor; further, dynamic tuning of the pre-designed optical properties of the PDMS lens (i.e., focal length, magnification) and NP filter (i.e., wavelength,

transmittance) can be performed by exposure to different solvents, besides hexane and diethyl ether.

We foresee the use of the proposed 4D printed NP-decorated PDMS lenses for a variety of lighting applications, such as color tuning, light filtering, and on-field microscopy applications, among which bacteria and pathogen detection on wounds, surface, and food, as well as water quality monitoring through protozoa and protists identification and quantification.

Eventually, the proposed 4D printing method can be also tailored to thin PDMS layers that can conform to geometries of existing lenses, therefore complementing existing dichroic filter elements made of glass substrates that cannot conform to surfaces.

### Supporting Information

Supporting Information is available from the Wiley Online Library or from the author.

### Acknowledgements

S.M. and M.C. contributed equally to this work. G.B. acknowledges the support of Italian Ministry of Education, University and Research (MIUR) in the framework of the CrossLab project (Departments of Excellence).

Open Access Funding provided by Universita degli Studi di Pisa within the CRUI-CARE Agreement.

### Conflict of Interest

The authors declare no conflict of interest.

### Data Availability Statement

Research data are not shared.

### Keywords

4D printing, fluorescence microscopy, lighting applications, nanoparticles, PDMS lenses, plasmonic nanoparticles, porous silicon, protists

Received: August 4, 2021

Revised: October 27, 2021

Published online:

- [1] Z. S. Ballard, C. Brown, A. Ozcan, *ACS Nano* **2018**, *12*, 3065.
- [2] H. C. Koydemir, A. Ozcan, *Future Microbiol.* **2017**, *12*, 641.
- [3] D. Tseng, O. Mudanyali, C. Oztoprak, S. O. Isikman, I. Sencan, O. Yaglidere, A. Ozcan, *Lab Chip* **2010**, *10*, 1787.
- [4] Q. Wei, H. Qi, W. Luo, D. Tseng, S. J. Ki, Z. Wan, Z. Göröcs, L. A. Bentolila, T.-T. Wu, R. Sun, A. Ozcan, *ACS Nano* **2013**, *7*, 9147.
- [5] S. Mariani, V. Robbiano, R. Iglio, A. A. La Mattina, P. Nadimi, J. Wang, B. Kim, T. Kumeria, M. J. Sailor, G. Barillaro, *Adv. Funct. Mater.* **2020**, *30*, 1906836.
- [6] W. M. Lee, A. Upadhy, P. J. Reece, T. G. Phan, *Biomed. Opt. Express* **2014**, *5*, 1626.

- [7] R. Amarit, A. Kopwithhaya, P. Pongsoon, U. Jarujareet, K. Chaitavon, S. Porntheeraphat, S. Sumriddetchkajorn, T. Koanantakool, *PLoS One* **2016**, *11*, e0146414.S.
- [8] S. Ekgasit, N. Kaewmanee, P. Jangtawee, C. Thammacharoen, M. Donphoongpri, *ACS Appl. Mater. Interfaces* **2016**, *8*, 20474.
- [9] B. Dai, Z. Jiao, L. Zheng, H. Bachman, Y. Fu, X. Wan, Y. Zhang, Y. Huang, X. Han, C. Zhao, T. J. Huang, S. Zhuang, D. Zhang, *Light: Sci. Appl.* **2019**, *8*, 75.
- [10] S. Mariani, A. A. La Mattina, A. Paghi, L. Strambini, G. Barillaro, *Adv. Funct. Mater.* **2021**, *31*, 2100774.
- [11] Q. Zhang, J.-J. Xu, Y. Liu, H.-Y. Chen, *Lab Chip* **2008**, *8*, 352.
- [12] X. Kuang, D. J. Roach, J. Wu, C. M. Hamel, Z. Ding, T. Wang, M. L. Dunn, H. J. Qi, *Adv. Funct. Mater.* **2019**, *29*, 1805290.
- [13] Y. Xia, Y. He, F. Zhang, Y. Liu, J. Leng, *Adv. Mater.* **2021**, *33*, 2000713.
- [14] D. N. Hupalo, M. Bradic, J. M. Carlton, *Curr. Opin. Microbiol.* **2015**, *23*, 49.
- [15] G. Whyman, E. Bormashenko, T. Stein, *Chem. Phys. Lett.* **2008**, *450*, 355.
- [16] V. A. Lubarda, K. A. Talke, *Langmuir* **2011**, *27*, 10705.
- [17] J. N. Lee, C. Park, G. M. Whitesides, *Anal. Chem.* **2003**, *75*, 6544.
- [18] W. F. Diller, D. Kounaris, *Biol. Bull.* **1966**, *131*, 437.
- [19] K. Ivan, V. Katya, *J. Biol. Sci. Opin.* **2014**, *2*, 298.